FARMER LABS / PLANETARY DEFENCE

ARGUS-PD/POD-7K Paper III

Coupled Feasibility Boundaries, Uncertainty Propagation and Falsification Criteria

Christopher I. V. Farmer

Series Paper III • Independent preprint for technical review

JULY 2026

coupled closure • uncertainty • evidence ladder • falsification

Abstract

This capstone paper replaces the earlier narrative series synthesis with a reproducible parametric closure of the ARGUS-PD/POD-7K research architecture. It asks a stricter question than whether the reference arithmetic is correct: under what combinations of moving mass, speed, coupling area, field bound, electrical efficiency, storage performance, structural reaction, release covariance and target-response uncertainty does a fixed seven-kilometre architecture remain expressible, and which measurement would force it to be reduced or abandoned?

The analysis establishes a controlled dependency graph. Complete moving mass sets kinetic energy and momentum. Energy over fixed length sets mean force. Force and a declared ideal field ceiling set minimum coupling area. Coupling area changes collar mass, which changes complete moving mass and therefore requires iteration. Efficiency sets admitted energy and waste. Specific energy and specific power produce independent lower bounds on storage mass. Momentum sets launcher reaction and, with uncertain target coupling, only a distribution of asteroid response. Angular, timing, target-state and model uncertainties combine into a release-and-impact covariance rather than a quoted accuracy.

The reference conservation identities survive audit: a 0.300 kg complete moving assembly at 10^6 m s^{-1} carries 150 GJ and 300 kN s; constant acceleration over 7,000 m gives 21.429 MN and 14 ms; an ideal 0.200 m^2 force surface corresponds to 16.410 T; and the assumed 35% efficiency plus 20% reserve corresponds to 514.286 GJ nameplate. The corrected mass ledger does not yet close experimentally. Its 0.090 kg, 0.200 m^2 collar implies 0.45 kg m^{-2} before representative force, thermal and release testing.

A computational grid and exact non-dominance test replace the previous claim of a universal optimum. Under a 150 GJ mechanical ceiling, speed and momentum form a Pareto frontier. Sensitivity is dominated algebraically by velocity ($E \propto v^2$), efficiency ($E_{admit} \propto \eta^{-1}$), length ($\acute{F} \propto L^{-1}$) and available field ($A_{min} \propto B^{-2}$). No present hardware establishes the full coupled solution. The paper therefore defines falsification thresholds at the level of the moving article, representative cell, pulse store, physical string, structure, release covariance and target response. The series is suitable for publication as an evidence-gated theoretical programme, not as a completed system or claim of engineering viability.

The closure also includes the external material column. Space is not a complete vacuum: meteoroid flux, residual gas and impact-generated plasma create stochastic flight-survival constraints, while atmospheric entry is an ablation and radiation-hydrodynamics problem. These variables do not alter the vacuum conservation identities; they can eliminate otherwise admissible projectile states.

Keywords: feasibility boundary; uncertainty propagation; falsification; Pareto analysis; systems engineering; planetary defence; reproducibility.

1. Purpose of the capstone

Papers I and II deliberately have different centres of gravity. Paper I asks which moving assemblies survive a coupled mass-speed-interface trade. Paper II asks what the fixed 7 km architecture demands of energy, pulse power, structure, thermal management, deployment and governance. A capstone is useful only if it adds analysis rather than repeating them.

This paper therefore owns five series-wide functions:

1. the controlled variables and dependencies;
2. the iterative mass-area-energy closure;
3. uncertainty propagation and sensitivity;
4. multi-objective design-space results; and
5. falsification and stop rules.

It also controls supersession. The current publication set is:

Series item	Controlling scope
Paper I	moving assembly, materials, coupling interface and Pareto trade
Paper II	fixed 7 km integrated architecture and verification programme
Paper III	dependencies, uncertainties, feasibility boundaries and falsification

The launcher science and application study is deposited separately rather than numbered as Paper IV. It tests a physical interpretation of the 6,000 module bays, quantifies the rear counter-impulse proposal, defines variable-energy scientific modes, models dust and atmospheric exposure scales, and applies the projectile frontier to generic target-size, distance and warning circumstances. Papers I-III remain the uniform sequential core.

The 49 km planetary-defence paper, the 98/392 km theoretical audit and the 1,001 km engineering paper are historical sources only. They are not alternate designs within the current series.

2. Controlled model

2.1 State vector

The minimum screening state is

$$x=\{m_i, v, L, A_c, B, \eta_e, r, \epsilon_E, \epsilon_P, M_p, \Sigma_{release}, \Sigma_{target}, \Phi_d, \Sigma_g, M, F, \beta, M_a\}. \quad (1)$$

Here m_i are the moving-mass components, ϵ_E and ϵ_P are installed usable specific energy and pulse power, M_p is the platform mass, the covariance matrices describe release and target state, β is uncertain momentum enhancement and M_a target mass. Φ_d represents trajectory-dependent dust flux, Σ_g the residual-gas or atmospheric column, and M the candidate-specific material state, including concentration, microstructure, temperature and interfaces. F is its statistical flaw population. The candidates include CVD diamond, BDD, diamond-SiC, toughened SiC, boron carbide, tungsten and carbon-rich sacrificial architectures; no member is preselected [14]. Variables absent from Eq. (1) may still be essential to engineering, but no series-wide viability claim can omit any term shown.

The external-state terms are evidence-linked rather than decorative: MEM3 supplies a trajectory-conditioned meteoroid environment [10]; measured BDD softening prevents a universal material constant [11]; spacecraft impact detection supports the plasma and charge observables [12]; and high-speed sample-return modelling establishes why atmospheric entry requires a coupled aerothermodynamic treatment [13].

2.2 Conservation layer

$$m=\sum_i m_i, E_k=\frac{1}{2}mv^2, p=mv. \quad (2)$$

$$a=\frac{v^2}{2L}, t_L=\frac{2L}{v}, \acute{F}=\frac{E_k}{L}. \quad (3)$$

These equations are exact for the declared constant-acceleration screen. They do not model cell ripple or structural transient.

2.3 Energy and thermal layer

$$E_{admit}=\frac{E_k}{\eta_e}, E_{nameplate}=(1+r)E_{admit}. \quad (4)$$

If a fraction f_{rec} of non-kinetic energy is recovered,

$$E_w = \left(1 - f_{rec}\right)\left(E_{admit} - E_k\right) + E_{aux}, \quad (5)$$

where E_{aux} includes cryogenic, control and conversion losses not already in the measured efficiency boundary. Equation (5) prevents double counting: the efficiency measurement and auxiliary ledger must share a declared system boundary.

2.4 Force-area-field layer

$$B_{ideal} = \sqrt{\frac{2\mu_0 E_k}{L A_c}}, A_{c,min} = \frac{2\mu_0 E_k}{L B_{max}^2}. \quad (6)$$

This is an ideal Maxwell-pressure screen. The topology layer must separately provide a circuit-derived force such as

$$F_x \simeq I_s I_a \frac{dM}{dx} + \frac{1}{2} I_a^2 \frac{dL_a}{dx}, \quad (7)$$

with measured losses, stability and reaction.

2.5 Storage and structure lower bounds

A candidate store must satisfy both:

$$m_{store} \geq \frac{E_{nameplate}}{\epsilon_E}, m_{store} \geq \frac{P_{pulse}}{\epsilon_P}. \quad (8)$$

These are lower bounds before containment, switching, thermal control, redundancy and qualification. A component that satisfies one inequality may fail the other.

Launcher reaction is

$$\Delta v_p = \frac{p}{M_p}. \quad (9)$$

No internal field symmetry removes Eq. (9). An external impulse, counter-mass, momentum exchange with another body or accepted orbit change is required.

A rear valve closes Eq. (9) only when it is treated as an external momentum-export device. If expelled mass m_e leaves at effective speed u_e, its opposed impulse is $m_e u_e$; residual platform velocity is $\left(p - m_e u_e\right) / M_p$. This validates the mechanism without deleting the structural reaction. For the 3 MN s T-DART member and a 2,000 t platform, uncompensated Δv_p is 1.5 m s^{-1}. Ideal matching at 4.5 km s^{-1}

consumes 666.7 kg per shot and requires a declared tolerance on impulse magnitude, direction and timing. The companion launcher study provides the reproducible screen [9].

The same study refines the 6,000-tranche proposition. Six thousand physical module bays are an admissible architectural hypothesis if each is a fault-contained multi-component chain or a local interface to shared bulk storage. No evidence identifies 6,000 existing single-component 85.714 MJ/0.51-5.10 GW modules.

3. The iterative closure that earlier drafts omitted

3.1 Why one pass is insufficient

The coupling area required by Eq. (6) has physical mass. If the collar areal density is σ_c,

$$m_{collar} = \sigma_c A_c + m_{edge} + m_{release}. \tag{10}$$

But m_{collar} appears inside total mass m, which appears in E_k, which determines A_c. The closure is therefore implicit:

$$A_c \geq \frac{\mu_0 v^2}{L B_{max}^2}\left(m_{fixed} + \sigma_c A_c\right). \tag{11}$$

Solving Eq. (11) gives

$$A_c \geq \frac{\mu_0 v^2 m_{fixed} / \left(L B_{max}^2\right)}{1 - \mu_0 v^2 \sigma_c / \left(L B_{max}^2\right)}, \tag{12}$$

provided the denominator is positive. If

$$\Pi_c = \frac{\mu_0 v^2 \sigma_c}{L B_{max}^2} \geq 1, \tag{13}$$

no finite collar area closes within the ideal screen for that fixed mass, speed, length, field and areal density. Π_c is a useful feasibility parameter: it converts a vague concern about collar mass into a falsifiable boundary.

For the present reference, $\sigma_c = 0.45$ kg m^{-2}, $v = 10^6$ m s^{-1}, $L = 7{,}000$ m and $B_{max} = 16.5$ T give $\Pi_c \approx 0.297$. Ideal closure is therefore mathematically possible, but not comfortably: at that value the collar's own mass is a first-order term in the area it demands, not a correction to it. The published 0.200

m^2 area is retained as a controlled allocation, not the result of a detailed collar design. A measured areal density substantially above the allocation must trigger a full iteration.

3.2 Reference mass ledger

Term	Value (kg)
Core	0.150
Functional skin	0.015
Load spreader	0.020
Coupling collar	0.090
Guidance/telemetry	0.010
Release interface	0.010
Other moving	0.005
Total	**0.300**

The allocation is falsified if a representative assembly cannot be weighed at or below 0.300 kg while retaining the declared area and functions. No prose exception is permitted.

4. Exact sensitivity of the shared equations

Logarithmic sensitivities expose the dominant multipliers. For $E_k = 1/2\, m v^2$,

$$\frac{\partial \ln E_k}{\partial \ln m} = 1, \frac{\partial \ln E_k}{\partial \ln v} = 2. \tag{14}$$

For the ideal field,

$$\frac{\partial \ln B}{\partial \ln m} = \frac{1}{2}, \frac{\partial \ln B}{\partial \ln v} = 1, \frac{\partial \ln B}{\partial \ln L} = -\frac{1}{2}, \frac{\partial \ln B}{\partial \ln A_c} = -\frac{1}{2}. \tag{15}$$

For required area at fixed field,

$$\frac{\partial \ln A_{c,min}}{\partial \ln m} = 1, \frac{\partial \ln A_{c,min}}{\partial \ln v} = 2, \frac{\partial \ln A_{c,min}}{\partial \ln L} = -1, \frac{\partial \ln A_{c,min}}{\partial \ln B_{max}} = -2. \tag{16}$$

For admitted energy,

$$\frac{\partial \ln E_{admit}}{\partial \ln \eta_e} = -1. \quad (17)$$

The implications are immediate:

- speed is the most severe direct multiplier of energy and area;
- a 10% efficiency shortfall raises admitted energy and first-order waste by about 11.1% when changing from 0.35 to 0.315;
- a 10% field shortfall requires about 23.5% more area; and
- extra length reduces force and area but does not reduce final kinetic energy.

Sensitivity does not show uncertainty probability. It shows where measurement quality matters most.

5. Uncertainty propagation

5.1 Measurement and model categories

The series distinguishes:

- **aleatory uncertainty:** variability such as manufacturing tolerances or uncertain target material;
- **epistemic uncertainty:** incomplete knowledge such as unvalidated impact physics;
- **assumption uncertainty:** values selected for study, including 35% efficiency; and
- **model-form uncertainty:** discrepancy between ideal equations and the real topology.

Quoting more decimal places does not reduce any category.

5.2 First-order propagation

For outputs $y = f(x)$, a local covariance approximation is

$$\Sigma_y \simeq J \Sigma_x J^T + \Sigma_{model}, J_{ij} = \frac{\partial f_i}{\partial x_j}. \quad (18)$$

The model-discrepancy term is mandatory when ideal pressure, constant force or line-of-flight time stands in for physical dynamics.

5.3 Release and target covariance

A transparent scalar screen is

$$\sigma_{miss}^2 = (R \sigma_\theta)^2 + (v \sigma_t)^2 + \sigma_{target}^2 + \sigma_{transfer}^2 + \sigma_{model}^2. \quad (19)$$

Equation (19) is not a mission design. It prevents the series from replacing a covariance with an unsupported accuracy claim. At a fixed range, angular error does not improve merely because speed rises. Timing sensitivity becomes worse in distance per unit time.

5.4 Target response

$$\Delta v_a = \frac{\beta m v_{rel}}{M_a}. \tag{20}$$

β, M_a, impact angle, local topography, porosity and fragmentation are uncertain and often correlated. DART provides measured evidence for one binary-asteroid experiment [1-4]; it does not provide a universal β or validate the extreme-speed regime. A mission-level claim requires a distribution of outcomes and a safe-fragment criterion, not Eq. (20) alone.

5.5 Material and particulate-flight survival

The external material column introduces a coupled aleatory/epistemic problem. Meteoroid arrival is stochastic; the critical damage threshold is material-, flaw- and model-form dependent. Solar Probe Plus/Parker Solar Probe work provides a configuration-specific 7-150 km s^{-1} ballistic-limit workflow [15], and relativistic-probe research treats cumulative crater, melting and erosion effects [16]. Neither supplies an ARGUS ballistic limit. CVD-diamond measurements also show that toughness and modulus vary with microstructure [17,18], so undoped thin-film properties are not BDD allowables.

For a critical population supplied by a trajectory-specific environment model, the uniform sensitivity form is

$$\lambda = A_p n_{\geq m_*} D, P(N \geq k) = 1 - e^{-\lambda} \sum_{j=0}^{k-1} \frac{\lambda^j}{j!}. \tag{20a}$$

At 50 mm projected diameter, a 50% chance of at least one critical hit corresponds to $n_{\geq m_*} = 3.53 \times 10^{-4}$, 3.53×10^{-7} and 2.36×10^{-9} m^{-3} over 1,000 km, 1,000,000 km and 1 au. These are inverse-probability thresholds, not estimates of space-dust number density. The particle distribution must be transformed into the projectile frame.

Repeated subcritical events require a compound damage state,

$$D = \sum_i \psi(m_i, v_{r,i}, x_i, \theta_i; M, F), P_{fail} = P(D \geq 1), \tag{20b}$$

with ψ calibrated to crater overlap, erosion, charge, angular impulse, stress-wave interaction and crack coalescence. The Paper I surface-creation-energy calculation is a conservative trigger for those tests, not a substitute for ψ, a hydrocode or a ballistic-limit experiment.

6. Multi-objective boundary

6.1 Computed design grid

The deposit code evaluates a grid across:

$$0.300 \le m \le 30\,kg,\ 100 \le v \le 1{,}000\,km\,s^{-1}, \quad (21)$$

under the 150 GJ mechanical ceiling and fixed 7 km length. It computes energy, momentum, installed nameplate, required area at 16.5 T, circular-equivalent diameter, $0.5\,AU/v$ and a declared covariance screen.

The exact non-dominance test maximises speed and momentum. Twenty-eight discrete points remain on the computed frontier; the machine-readable CSV preserves them without rounding.

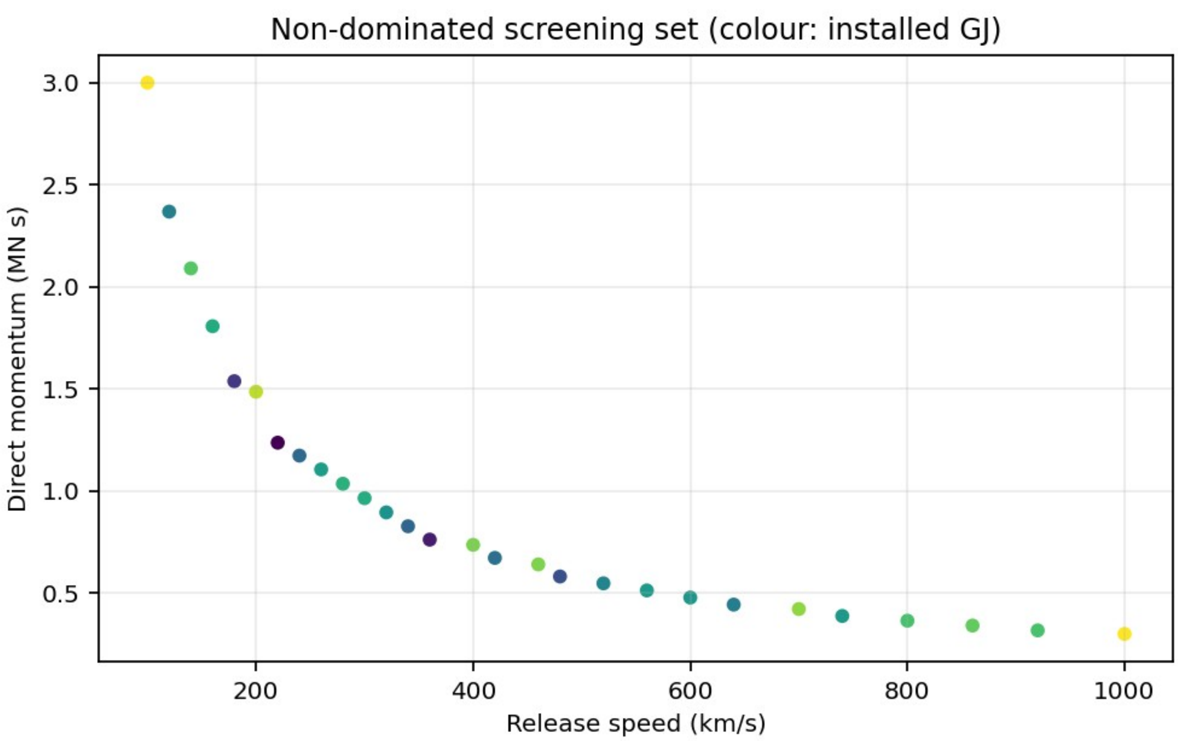

Computed non-dominated screening set. The frontier is a numerical result of the declared grid and constraints, not an operational mission recommendation.

6.2 Interpretation

At fixed energy,

$$p = \frac{2E}{v}. \tag{22}$$

The speed-momentum conflict is therefore structural. A unique “best projectile” exists only after the decision-maker supplies warning time, minimum impulse, uncertainty, target response, safety and technology constraints. The series uses three research decision rules:

1. **rapid-response screen:** maximise speed subject to all hard constraints;
2. **coherent-impulse screen:** maximise momentum subject to arrival time; and
3. **balanced screen:** impose minimum speed and momentum, then minimise installed energy, coupling area and evidence burden.

The labels R-, V-, M- and T-DART are convenient points, not evidence that a member should be built.

7. Coupled feasibility boundaries

7.1 Boundary table

Boundary	Mathematical or evidentiary condition	Consequence of failure
Moving mass	representative article $m \le m_{declared}$	recompute all outputs
Collar feedback	$\Pi_c < 1$ with margin	reduce speed, increase length/field or change interface
Field screen	$B_{ideal} \le B_{declared}$	area or force must change
Topology	measured circuit force and stability match duty	ideal pressure cannot support claim
Efficiency	measured η_e within accepted band	storage and thermal design grow
Storage energy	Eq. (8) energy bound closes	reduce shot or reject architecture
Storage power	Eq. (8) power bound closes	change pulse concept or reject
Reaction	external momentum strategy closes	no free-platform operation
Release covariance	target-independent test bound achieved	no mission analysis
Flight environment	material-specific critical-hit and compound damage probability meet requirement	reduce speed, change article or reject trajectory

Boundary	Mathematical or evidentiary condition	Consequence of failure
Atmospheric column	no intact Earth-atmosphere state is claimed	treat as energy deposition or exclude
Target response	validated outcome distribution	no effectiveness claim
Governance	target-specific civil authorisation	no operation

7.2 Evidence states

Each proposition is assigned one state:

- **E0—identity:** follows from controlled equations;
- **E1—analogue:** a relevant material or component effect exists;
- **E2—representative:** a scaled article has met the relevant combined duty;
- **E3—integrated:** the subsystem has met interfaces and faults in context;
- **E4—mission:** target-specific, safe and authorised performance is shown.

The reference energy arithmetic is E0. Static REBCO field magnitude is E1. The moving collar, representative force cell and pulse store are below E2. No E3 or E4 claim is made.

8. Falsification plan

8.1 Quantitative stop rules

The following are intentionally capable of ending the reference architecture:

1. a weighed 0.200 m^2 moving interface cannot meet the 0.090 kg allocation or a revised iterative mass solution;
2. a representative cell cannot produce the required normalised force at acceptable stability and efficiency;
3. extrapolated storage mass from demonstrated ϵ_E and ϵ_P is incompatible with deployment;
4. pulse or quench faults cannot be contained within a bounded cell domain;
5. transient structural response cannot preserve clearance and centreline;
6. release covariance remains incompatible with any safe research range;
7. no candidate material architecture and particle-frame trajectory exposure can establish acceptable Poisson critical-hit and compound-damage probabilities;
8. extreme-speed impact models cannot be validated sufficiently to bound fragmentation; or
9. no lawful civil authorisation and oversight structure can be established.

8.2 Gate sequence

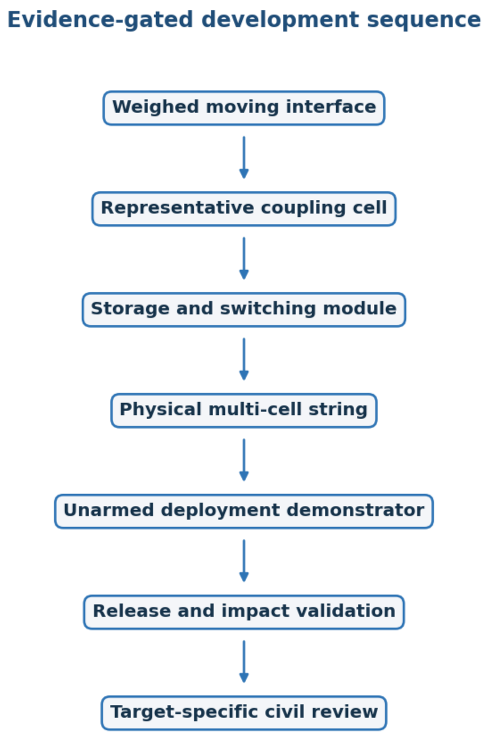

Evidence-gated development sequence. Each later stage depends on evidence from the preceding stage.

No later gate can repair a failed earlier gate by assertion. Gate order may be parallelised for research efficiency, but evidence inheritance remains one-way. This requirements-to-verification logic follows the systems-engineering distinction between analytical closure, component verification and integrated validation [5].

9. Reproducibility and claim ownership

The publication package contains:

- the controlled Python model;
- twenty-one unit tests covering reference arithmetic, field screening, moving mass, core geometry, uncertainty monotonicity, geomagnetic bounds, a loop calculation, physical module duty, rear counter-impulse, scenario scale and warning-distance inversion, variable-energy scaling, flight-environment screens, dust fracture and encounter statistics, and the programme-cost model;
- the complete parametric grid;

- the non-dominated frontier;
- the reference family and mass ledger;
- module-duty, counter-impulse, operating-mode, application-utility, material-evidence, dust-collision, dust-fracture, dust-encounter, flight-environment, warning-distance and asteroid-scenario screening tables;
- figure-generation code;
- a low-degree IGRF-14 companion calculation;
- provenance and checksums; and
- a claim-to-source and archive manifest.

The package does **not** claim to contain mission trajectories, electromagnetic finite-element solutions, detailed switching designs, structural finite-element models, quench simulations or impact hydrocodes. Those remain evidence gates. The availability statement is therefore verifiable rather than aspirational.

10. Limitations

The most consequential limitation is model form. Constant force, uniform Maxwell pressure, deterministic efficiency and R/v flight time are screening abstractions. The design grid is intentionally non-operational and does not optimise trajectories or target solutions. The IGRF calculation belongs to a separate attitude-control paper and is not evidence that an interplanetary installation can use geomagnetic control.

The parameter ranges do not imply that endpoints are technically reachable. They define the space in which contradictions and sensitivities are exposed. The static trapped-field comparator [6] and the impact-scaling literature [7,8] constrain different edges of the problem; neither validates the coupled architecture. Experimental data may shrink the space to zero.

11. Series adjudication and conclusion

The corrected series has a defensible but narrow affirmative result:

- the reference conservation arithmetic is internally consistent;
- the moving-mass contradiction has been made explicit and corrected as a controlled allocation;
- the ideal collar-area result is reproducible and properly bounded;
- the speed-momentum trade is a genuine Pareto problem;

- material selection and particulate-flight survival are now explicit stochastic evidence gates rather than assumed BDD properties;
- the dependencies and stop rules are finite; and
- the claimed data and code now exist.

The series does not establish that a 7 km extreme-velocity system can be built. It does not establish present storage, dynamic coupling, structural life, release accuracy, target effect, system mass, cost, schedule or mission authorisation. A DOI would make this version persistently identifiable; it would not supply peer review or elevate its evidence state.

The research is complete only in the limited manuscript sense that its central hypothesis, assumptions, equations, dependencies, uncertainties and falsification criteria are explicit. Empirical closure remains the substance of the proposed programme.

Declarations

Funding. No external funding is declared.

Competing interests. The author declares no competing financial interest.

Data and code availability. The computational screening package, tests, tables, figures and provenance record accompany this paper.

Dual-use boundary. No operational trajectory, target solution, firing logic, command architecture or terrestrial/anti-satellite use is included.

References

1. Adams, E. et al. *Final DART Technical Report to NASA*. NASA NTRS 20230015804 (2023). https://ntrs.nasa.gov/citations/20230015804.
2. Daly, R. T. et al. Successful kinetic impact into an asteroid for planetary defence. *Nature* 616, 443-447 (2023). https://doi.org/10.1038/s41586-023-05810-5.
3. Cheng, A. F. et al. Momentum transfer from the DART mission kinetic impact on asteroid Dimorphos. *Nature* 616, 457-460 (2023). https://doi.org/10.1038/s41586-023-05878-z.
4. Thomas, C. A. et al. Orbital-period change of Dimorphos due to the DART kinetic impact. *Nature* 616, 448-451 (2023). https://doi.org/10.1038/s41586-023-05805-2.
5. NASA. *Systems Engineering Handbook*, NASA/SP-2016-6105 Rev. 2 (2016).
6. Patel, A. et al. A trapped field of 17.7 T in a stack of high-temperature superconducting tape. *Superconductor Science and Technology* 31, 09LT01 (2018). https://doi.org/10.1088/1361-6668/aad34c.
7. Holsapple, K. A. & Housen, K. R. Momentum transfer in asteroid impacts: theory and scaling. *Icarus* 221, 875-887 (2012). https://doi.org/10.1016/j.icarus.2012.09.022.
8. Raducan, S. D. et al. Influence of projectile geometry on momentum transfer and implications for DART. *International Journal of Impact Engineering* 162, 104147 (2022). https://doi.org/10.1016/j.ijimpeng.2021.104147.
9. Farmer, C. I. V. *ARGUS-PD/POD-7K Launcher Science and Application Envelope: Distributed Pulse-Module Architecture, Counter-Impulse Closure, Projectile-Family Physics and Space-Only Research Utility*. Version 1.0.0, companion preprint (2026).
10. Moorhead, A. V., Kingery, A. & Ehlert, S. NASA's Meteoroid Engineering Model 3 and its ability to replicate spacecraft impact rates. *Journal of Spacecraft and Rockets* 57 (2020). https://ntrs.nasa.gov/citations/20200000563.
11. Liu, X. et al. Elastic and mechanical softening in boron-doped diamond. *Scientific Reports* 7, 42921 (2017). https://doi.org/10.1038/srep42921.
12. Lee, N. & Close, S. Meteoroid impact detection for exploration of asteroids: small satellites for asteroid characterization. *Journal of Spacecraft and Rockets* 55 (2018). https://doi.org/10.2514/1.A33928.
13. Johnston, C. O. Study of aerothermodynamic modeling issues relevant to high-speed sample return vehicles. NATO STO-AVT-218 (2014). https://ntrs.nasa.gov/citations/20140004052.

14. Farmer, C. I. V. *ARGUS-PD/POD-7K Paper I: Parametric Design-Space Analysis of a Modular Projectile Family and Electromagnetic Launch Interface*. Version 1.1.0, companion preprint (2026).
15. Iyer, K. A., Mehoke, D. S. & Batra, R. C. Interplanetary dust particle shielding capability of spacecraft multilayer insulation. *Journal of Spacecraft and Rockets* 52, 584-594 (2015). https://doi.org/10.2514/1.A33101.
16. Hoang, T., Lazarian, A., Burkhart, B. & Loeb, A. The interaction of relativistic spacecrafts with the interstellar medium. *Astrophysical Journal* 837, 5 (2017). https://doi.org/10.3847/1538-4357/aa5da6.
17. Drory, M. D., Dauskardt, R. H., Kant, A. & Ritchie, R. O. Fracture of synthetic diamond. *Journal of Applied Physics* 78, 3083-3088 (1995). https://doi.org/10.1063/1.360060.
18. Meindlhumer, M. et al. Micromechanical properties of micro- and nanocrystalline CVD diamond thin films with gradient microstructures and stresses. *Journal of Vacuum Science & Technology A* 42, 023401 (2024). https://doi.org/10.1116/6.0003235.